



Crack propagation in pre-strained single layer graphene sheets



Minh-Quy Le^{a,b}, Romesh C. Batra^{c,*}

^aDepartment of Mechanics of Materials, School of Mechanical Engineering, Hanoi University of Science and Technology, No. 1 Dai Co Viet Road, Hanoi, Viet Nam

^bInternational Research Center for Computational Materials Science, Hanoi University of Science and Technology, No. 1 Dai Co Viet Road, Hanoi, Viet Nam

^cDepartment of Engineering Science and Mechanics, M/C 0219, Virginia Polytechnic Institute and State University, Blacksburg, VA 24061, USA

ARTICLE INFO

Article history:

Received 13 August 2013

Received in revised form 25 November 2013

Accepted 2 December 2013

Keywords:

Crack propagation

Graphene sheet

Molecular dynamics simulations

J-integral

ABSTRACT

We use molecular dynamics simulations to delineate crack propagation speed as a function of the crack length and the axial prestrain in a single layer graphene sheet. A covalent bond between two carbon atoms is assumed to break when the bond length has been stretched by 100%. For a pristine single layer graphene sheet the maximum axial force is attained at a nominal axial strain of 15.5%. A pristine graphene sheet is first deformed in tension in the armchair direction to the desired value of the axial strain, and then one or two cracks are simultaneously inserted in it at central locations by breaking the bonds. Five such problems have been studied with four different values of the axial prestrain up to 15.3%. For each problem, crack-tip speeds are found to reach steady state values as the crack elongates. The steady state crack speed increases with an increase in the axial nominal prestrain. The crack propagation is found to be stable in the sense that the value of the *J*-integral increases with an increase in the crack length. For the same normalized crack length the value of the *J*-integral increases with an increase in the nominal axial prestrain.

© 2013 Elsevier B.V. All rights reserved.

1. Introduction

Single layer graphene sheets (SLGSs) and nano-composites with graphene sheets as reinforcements have in general superior mechanical [1], thermal [2], and electronic [3] properties than many other monolithic and composite materials, and have potential applications in nano-electronic devices [4,5]. Needless to say, the fracture of graphene plays a significant role in designing graphene based materials and structures. Several authors [6,7] have used linear elastic fracture mechanics approach to investigate crack initiation and propagation in SLGSs even though the mechanical response of a SLGS may be highly nonlinear (see e. g., [8]). Xu et al. [7] used a coupled quantum/continuum mechanics approach to study crack propagation in armchair and zigzag SLGSs with initial cracks perpendicular to zigzag and armchair edges. The crack growth was found to be self-similar in zigzag sheets but irregular in armchair sheets. The critical stress intensity factors were found to be 4.21 MPa $\sqrt{\text{m}}$ and 3.71 MPa $\sqrt{\text{m}}$ in zigzag and armchair graphene sheets, respectively.

The *J*-integral (e.g., see [9]), defined below by Eq. (1), is generally used as a fracture characterizing parameter in linear elastic fracture mechanics.

$$J = \int_{\Gamma} \left(W dy - \sigma_{ij} n_j \frac{\partial u_i}{\partial x} d\Gamma \right) \quad (1)$$

Here *W* is the strain energy density, σ_{ij} and u_i are the Cauchy stress and the displacement components, respectively, with respect of rectangular Cartesian coordinate axes, n_j is the component of the unit outward normal to the closed contour Γ surrounding the crack-tip, a repeated index implies summation over the range of the index, and the crack is aligned along the *x*-axis. A discrete form of Eq. (1) has been suggested for use at the atomic level by Nakatani et al. [10] for amorphous metals and by Jin and Yuan [11] and Khare et al. [12] for graphene sheets. Jin and Yuan [11] have developed a method to calculate the *J*-integral in specified atomic domains and studied stationary cracks in graphene sheets. Khare et al. [12] used a coupled quantum/molecular mechanical modeling to estimate the strain energy release rate (SERR) at the point of crack extension in a SLGS.

For linear and nonlinear elastic materials, the *J*-integral can also be computed from the relation

$$J = - \frac{d\Pi}{dA} \quad (2)$$

where Π is the potential energy and *A* the crack surface area ($A = at$; *a* and *t* are the crack length and the sheet thickness, respectively), or equivalently from the slope of the potential energy vs. the crack length curve since the sheet thickness is constant. An advantage of using Eq. (2) to find *J* is that no detailed information for the stress and the strain fields around the crack-tip is needed. Le and Batra [13] used Eq. (2) to compute the SERR in a graphene sheet with a single edge crack and deformed in simple tension, and found that the SERR strongly depends upon the initial crack length. They also

* Corresponding author. Tel.: +1 540 231 6051; fax: +1 540 231 4574.

E-mail address: rbatra@vt.edu (R.C. Batra).

studied the dependence of the crack speed upon the crack length, nominal axial strain rate and the number of layers in the graphene sheet.

Since initial cracks in armchair graphene sheets are perpendicular to the tensile load axis, it is simpler to simulate crack propagation in armchair sheets than that in zigzag sheets. Accordingly, crack propagation in armchair graphene sheets has been more often investigated [6,11,12,14].

Here we use Eq. (2) and results of molecular dynamics (MD) simulations to investigate crack propagation in a pre-strained armchair SLGS as a function of the initial crack length, crack location and the pre-strain. A crack is assumed to elongate when the bond length perpendicular to the crack becomes twice of its value in the initial relaxed and unloaded configuration. It is found that the steady state crack propagation speed increases with an increase in the axial nominal prestrain, and the crack propagation is stable in the sense that the SERR increases with an increase in the crack length. An interesting result is that for the pristine SLGS the axial load attains its maximum value at the nominal axial strain of 15.48%. However, the crack propagation is stable in the SLGS pre-strained up to an axial nominal strain of 15.3%. Two equally long cracks on the centerline of the SLGS start interacting with each other when the distance between their tips equals $8\sqrt{3} r_0$ where r_0 is the distance between two carbon atoms in the unloaded relaxed configuration.

2. Numerical procedure

2.1. Molecular mechanics potential function

We describe in this subsection the molecular mechanics potential used in this work. Short-range (or bonded) interactions between carbon atoms are modeled by the Morse potential, a quadratic function of the change in cosines of the angle between bonds, and a 2-fold torsion potential [15,16]; their expressions are given by Eqs. (3a), (3b), and (3c), respectively, and various symbols are shown in Fig. 1.

$$V_{ij}^{bond} = D_e [1 - e^{-\beta(r_{ij} - r_0)}]^2, \quad (3a)$$

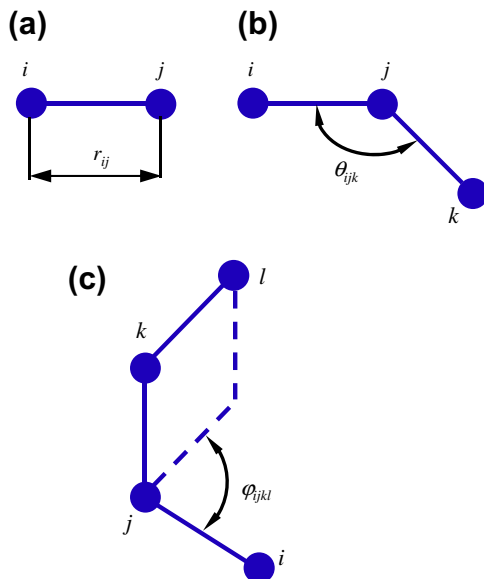


Fig. 1. Schematic illustration of (a) the bond length, (b) the angle θ_{ijk} between adjacent bonds, and (c) the torsional angle ϕ_{ijkl} .

$$V_{ijk}^{angle} = \frac{1}{2} K_\theta [\cos(\theta_{ijk}) - \cos(\theta_0)]^2, \quad (3b)$$

$$V_{ijkl}^{torsion} = \frac{1}{2} K_\phi [1 - \cos(2\phi_{ijkl})]^2. \quad (3c)$$

In Eqs. ((3a)–(3c)) and Eq. (4) below D_e , K_θ , K_ϕ , D_0 , and χ are material parameters. The Lennard–Jones potential given by Eq. (4) is adopted to describe the van der Waals interactions (long-range non-bonded interactions) between carbon atoms (e.g., see [17]).

$$V_{ij}^{vdw} = 4D_0 \left[\left(\frac{\chi}{r_{ij}} \right)^{12} - \left(\frac{\chi}{r_{ij}} \right)^6 \right] \quad (4)$$

Values of material parameters in Eqs. (1) through (4) taken from Walther et al. [16] and Girifalco et al. [17] are listed in Table 1. The total potential energy of all atoms in the system is given by:

$$V = \sum_{ij} V_{ij}^{bond} + \sum_{i,j,k} V_{ijk}^{angle} + \sum_{i,j,k,l} V_{ijkl}^{torsion} + \sum_{ij} V_{ij}^{vdw}. \quad (5)$$

We did not use any cut-off distance, thus interactions among all atoms in the system were considered.

2.2. Molecular dynamics simulations

MD simulations have been carried out for uniaxial tensile deformations of a pristine armchair $402.52 \text{ \AA} \times 398.92 \text{ \AA}$ SLGS containing 61,940 atoms with the freely available open-source software, LAMMPS, [18] in a microcanonical (NVE) ensemble with periodic boundary conditions. The temperature of the system is controlled at 0 K using a Langevin thermostat [19]. Initial velocities are randomly assigned to atoms, and they are allowed to relax without applying external loads for 50 ps using a time step of 1 fs. Subsequently, specimens are deformed at the axial strain rate of 10^8 s^{-1} by applying axial velocity in the armchair direction to atoms at the two ends of the specimen as schematically shown in Fig. 2. To study crack propagation, the pristine graphene sheet is first pre-strained in the armchair direction to the desired value of the axial strain, and then either one or two cracks are simultaneously inserted in the middle of the sheet by deleting bonds between atoms as shown in Fig. 3a through Fig. 3e. The crack length a is given by:

$$a = (n + 1)d \text{ for an interior crack (cases 1, 4 and 5),} \quad (6a)$$

$$a = \left(n + \frac{1}{2} \right) d \text{ for an edge crack (cases 2 and 3),} \quad (6b)$$

where n is number of consecutive broken bonds, $d = r_0\sqrt{3}$, and r_0 equals the distance between adjacent atoms in the relaxed configuration.

3. Uniaxial tensile deformations of a pristine single layer graphene sheet

The strain energy due to deformations of the structure is determined by subtracting the potential energy of the relaxed unloaded structure from that of the loaded structure. The evolution of the

Table 1
Values of parameters in the potential functions.

Interactions	Parameters
Bond-stretching	$D_e = 478.9 \text{ kJ/mol}$, $\beta = 2.1867 \text{ \AA}^{-1}$, $r_0 = 1.418 \text{ \AA}$
Angle bending	$K_\theta = 562.2 \text{ kJ/mol}$, $\theta_0 = 120^\circ$
Bond-torsion	$K_\phi = 25.12 \text{ kJ/mol}$
Lennard–Jones	$D_0 = 0.2313 \text{ kJ/mol}$, $\chi = 3.415 \text{ \AA}$

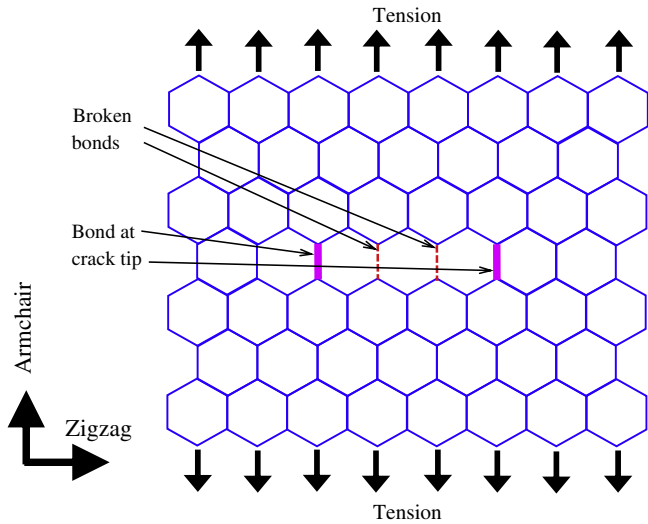


Fig. 2. Schematic sketch of the problem studied. A pristine single layer graphene sheet (SLGS) is pre-strained in uniaxial tension in the armchair direction, and a centered or single edge crack is inserted by deleting corresponding bonds.

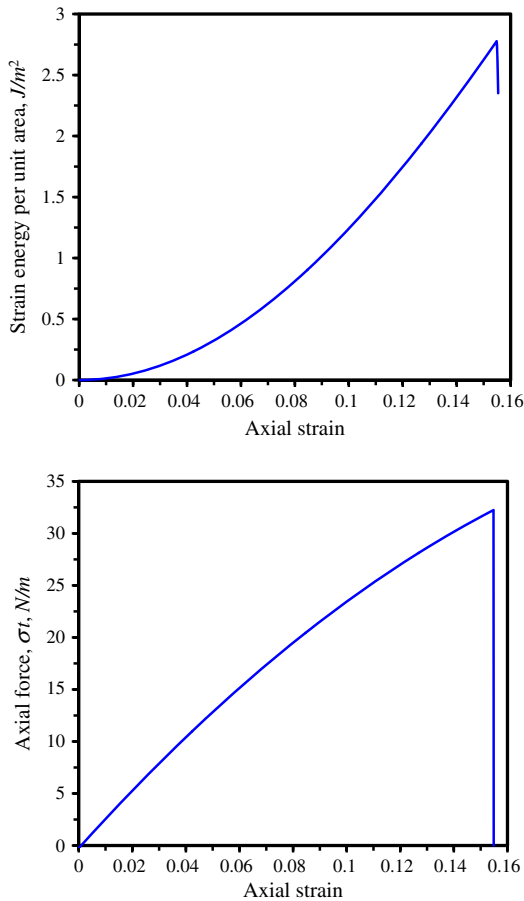


Fig. 3. Variation with the nominal axial strain of (top) strain energy per unit area, and (bottom) axial force in the pristine SLGS deformed in uniaxial tension in the armchair direction.

strain energy per unit volume, namely the strain energy density W , versus the nominal axial strain ε of the pristine SLGS is plotted in Fig. 3a. The lowest-order best-fit polynomial (with a correlation coefficient of 1.0) through the data is the following third-order expression

$$W = (-164.4\varepsilon^3 + 143.15\varepsilon^2 - 0.26\varepsilon)/t, \quad (7)$$

where t is the thickness of the SLGS in meters (Wt is strain energy per unit area of an edge face). The first derivative of W with respect to ε equals the nominal axial stress (see Fig. 4b) and the second derivative of W with respect to ε equals the elastic modulus E . We thus get

$$E = (-986.4\varepsilon + 286.3)/t \text{ N/m}^2. \quad (8)$$

That is, the modulus decreases with an increase in the axial strain and equals zero when the nominal axial strain equals 0.29.

At zero axial strain, $Et = 286.3 \text{ N/m}$ (or $E = 855 \text{ GPa}$ for $t = 3.35 \text{ \AA}$). This value is in good agreement with the experimental data of Lee et al. [1], phonon dynamics calculations of Liu et al. [20], DFT (Xu et al. [21]), and MD simulation results [22,23]. The summary of values of Et given in Table 1 of Gupta and Batra's [22] paper indicates that, depending upon the method used, it varies from 235 to 546 N/m with the experimental value determined from indentation tests between 290 and 390 N/m.

Poisson's ratio at small strains computed by taking the negative of the ratio of the average transverse strain to the average axial strain varies between 0.13 and 0.23 with an average value of 0.18. This value is close to 0.186 found by Liu et al. [20] using phonon dynamics, 0.169 reported by Wei et al. [8] employing the DFT, 0.22 obtained by Xu et al. [21], 0.21 found by Gupta and Batra [22] by using the MM3 potential, and 0.21 ± 0.01 computed by Zhao et al. [23] with the MD simulations using the Airebo potential. Needless to say, numerical values of material parameters derived from MM/MD simulations depend upon the potential used.

From the nominal axial stress vs. the nominal axial strain plot of Fig. 3b, we conclude that the nominal axial stress σ_f and the nominal axial strain ε_f at failure of the pristine SLGS equal $\sigma_f t = 32.2 \text{ N/m}$ ($\sigma_f \sim 96 \text{ GPa}$ for $t = 3.35 \text{ \AA}$) and $\varepsilon_f = 15.48\%$. These values are close to 90 GPa and 13%, respectively, found by Zhao et al. [23] using MD simulations with the Airebo potential, and 107 GPa and 20%, respectively, by Xu et al. [21] using the DFT.

4. Crack propagation

Several previous works considered a bond as broken when its length reached the cut-off distance of 2 \AA in the Tersoff–Brenner potential (e.g., see [11,12]). Xu et al. [7] in their quantum mechanics calculations identified broken bonds by a sharp decrease in the electron density at the bond midpoint and found that the bond is broken when its length is close to 2.9 \AA or approximately twice the initial length of 1.43 \AA . Here, as assumed in our earlier work [13], a bond is taken to be broken when its length equals 2.836 \AA . The corresponding bond stretching energy of 436.7 kJ/mol equals 91.2% of the depth $D_e = 478.9 \text{ kJ/mol}$ of the potential.

Five positions of initial cracks are considered as shown in Fig. 4, namely, a centered interior crack (case 1), a single edge crack (case 2), two edge cracks (case 3), an off-center interior crack (case 4), and two interior cracks symmetrically located about the SLGS centroid (case 5). The distance between the crack center and the sheet centroid in the zigzag direction is $1/4$ th of the sheet width for cases 4 and 5. It is found that crack faces remain perpendicular to the loading direction as a crack propagates straight ahead, see Figs. 4 and 5. We note that an initially uncracked pristine SLGS failed at a nominal axial strain of 15.48% which limits the maximum axial prestrain considered in this work.

4.1. Crack speed

Crack-tip speed v is determined from the relation:

$$v = \frac{da_t}{d\tau}, \quad (9)$$

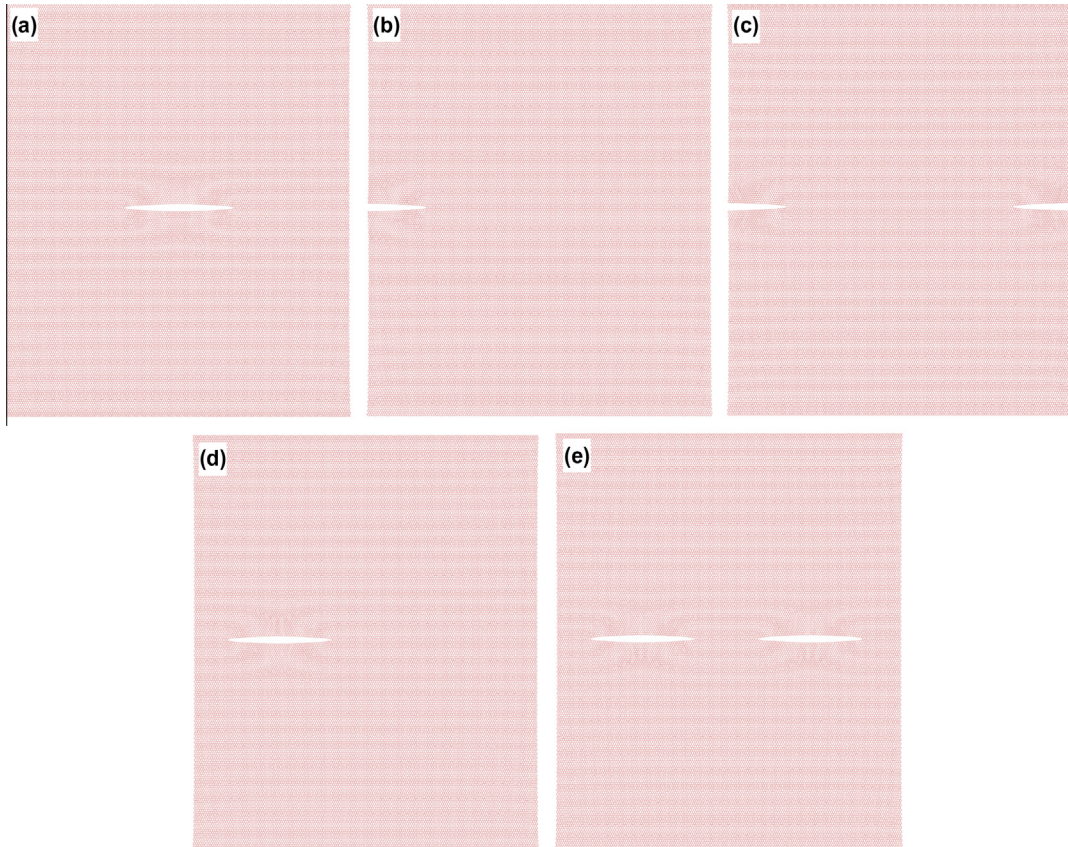


Fig. 4. Crack positions at 2 ps after inserting cracks at time = 0 in the SLGS prestrained to 15.3%. (a) An interior centered crack (case 1), (b) a single edge crack (case 2), (c) double edge cracks (case 3), (d) an interior crack offset from the centroid (case 4), and (e) two interior cracks symmetrically located about the centroid (case 5). For cases 4 and 5, the distance between the crack center and the sheet centroid in the zigzag direction equals $\frac{1}{4}$ th the sheet width.

where $d\tau$ is the time in which the crack-tip advances by distance da_τ . In our earlier work [13] we found that the computed potential energy and the J -integral values are essentially unaffected by the time step size $\Delta\tau$ provided that it is sufficiently small. However, the computed crack-tip speed is influenced by the time step size and the computed speed essentially converged for $\Delta\tau = 0.1$ fs. Here we have used the time step of 0.1 fs while studying crack initiation and propagation.

For an edge crack (cases 2 and 3), the crack speed equals the crack-tip speed. For interior cracks corresponding to cases 1 and 5, numerical simulations indicated that the two crack-tips propagate outwards at the same speed. For the interior cracks corresponding to case 4, the difference in speeds of the 2 crack-tips was found to be less than 3%, and has been neglected. Hence, the

rate of increase of the length of an interior crack equals twice the crack-tip speed. For an edge crack the crack speed equals the crack-tip speed. For case 4, when the distance between the left crack-tip and the free edge is about twice the lattice constant, the left crack-tip speed decreases due to the free edge effect.

For the centrally cracked SLGS, crack positions at 2, 4 and 6 ps are exhibited in Fig. 5. It is clear that the crack propagates symmetrically both to the left and the right of the vertical centerline.

For the single edge cracked and the centrally cracked SLGS we have plotted in Fig. 6 the crack-tip speed as a function of the normalized crack length, a/w , for four values, namely 8.4%, 10.7%, 13% and 15.3%, of the nominal axial prestrain. Here a and w equal, respectively, the present crack length and the SLGS width. These results evince that the crack-tip speed initially increases with an

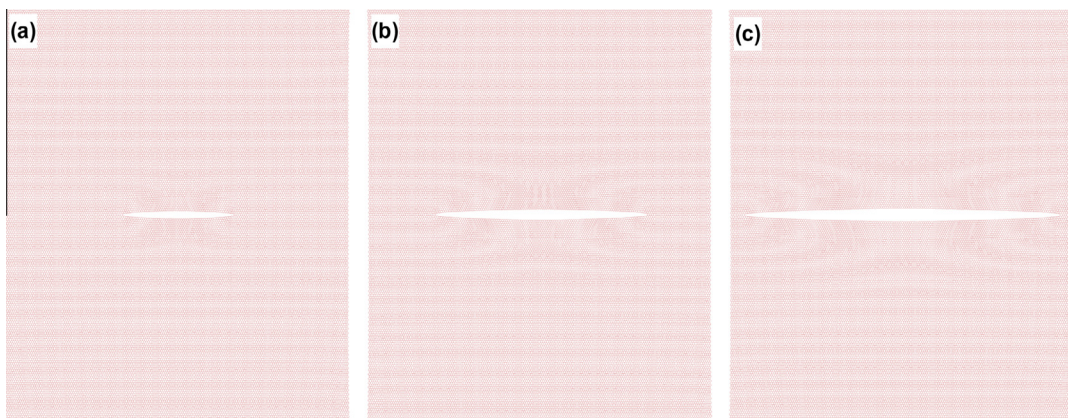


Fig. 5. For case (a), crack positions at (a) 2 ps, (b) 4 ps, and (c) 6 ps.

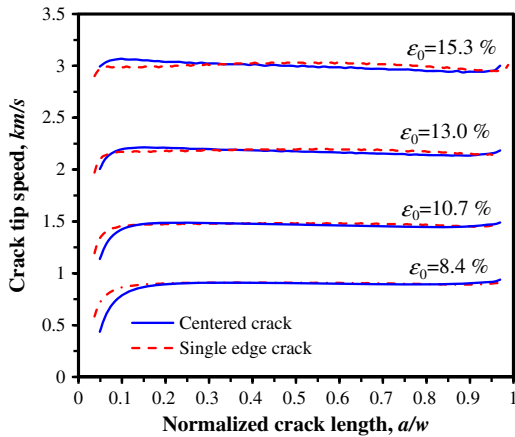


Fig. 6. For four values of the axial prestrain, dependence of the crack-tip speed upon the normalized crack length.

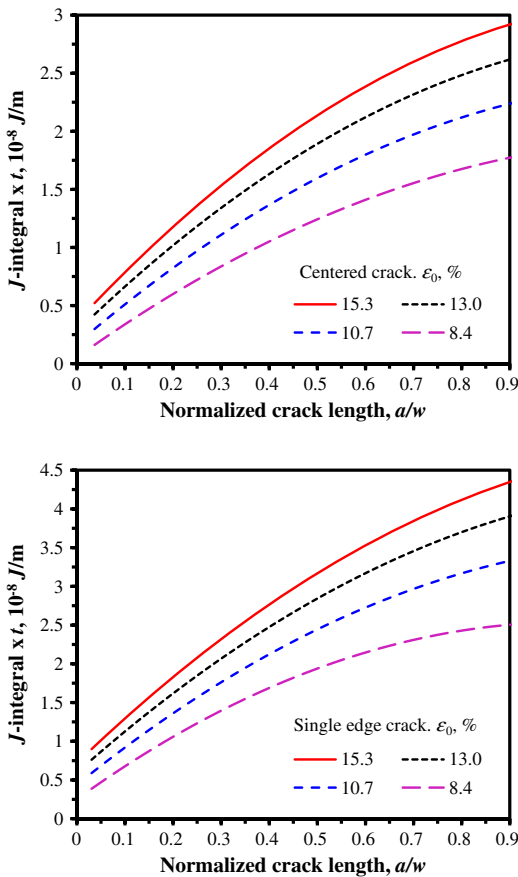


Fig. 7. Variation of the J -integral with the normalized crack length for four values of the axial prestrain, ϵ_0 , and (top) central interior cracked, and (bottom) single edge cracked SLGS.

increase in the value of a/w till a/w equals 0.2 and subsequently it stays constant. The initial as well as the steady state crack-tip speed increases with an increase in the value of the axial prestrain. For a given value of the prestrain, the steady state crack-tip speeds for the centrally and the edge-cracked SLGS are essentially the same. For the pre-strain of 15.3%, which is just below the fracture strain of 15.48%, the steady state crack-tip speed equals 3 km/s, and at a pre-strain of 8.4% it equals 0.9 km/s. It is interesting to note that even though results (sudden drop in the potential energy

at the axial strain of 15.48%) plotted in Fig. 3 suggest that the SLGS may become unstable when pulled beyond an axial strain of 15.48%, the insertion of a crack in the SLGS prestrained to 15.3% results in stable crack growth as indicated by the rising value of the J -integral (or the SERR) plotted in Fig. 7. These results also evince that for a given value of a/w , the SERR increases with an increase in the value of the prestrain irrespective of the location of the initial crack. Furthermore, for a given value of a/w and prestrain of 15.3%, the SERR is higher for the single-edge cracked graphene sheet than that for the center-cracked SLGS. Said differently, the SLGS exhibits rising J resistance curve, and a single toughness value cannot be specified as was also the case for a pre-cracked SLGS deformed in tension [13]. The SERR for the SLGS prestrained to 15.3% is higher than that for the SLGS with no prestrain.

For the nominal axial prestrain of 15.3%, we have exhibited in Fig. 8 the crack-tip speed versus a/w for the five locations of initial cracks, and for two crack lengths of centrally cracked and edge cracked SLGSs. These plots reveal that the steady state crack speeds are essentially independent of the initial crack length and location. For an initially unstrained SLGS deformed in simple tension, Le and Batra [13] have reported that the crack speed v strongly depends on the initial crack length, and with an increase in the crack length the crack speed first increases, reaches a maximum value and then decreases. The crack length at which the crack speed reaches the maximum value depended upon the length of the initial crack. We note that the existence of speed gap (i.e., the crack-tip speed essentially starting from a finite value) was pointed out earlier

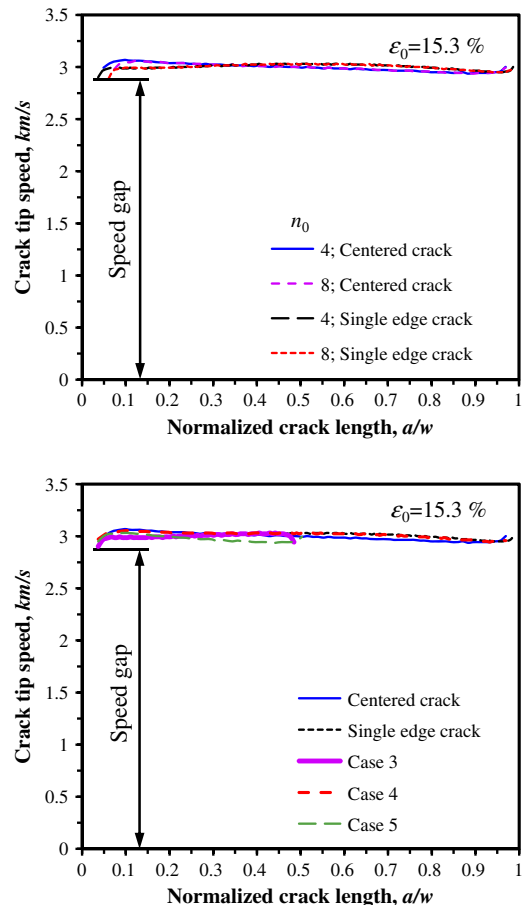


Fig. 8. For axial pre-strain of 15.3% variation of the crack-tip speed with the normalized crack length for (top) two values of the initial crack length and the crack located either at the centroid or at an edge of the SLGS, and (bottom) three locations of initial cracks, i.e., cases 3, 4 and 5.

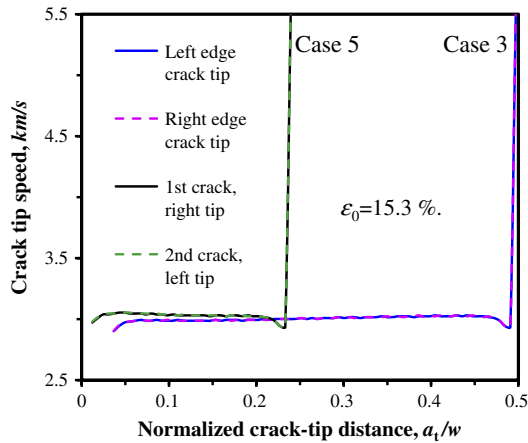


Fig. 9. Variation with the normalized crack-tip distance of the crack-tip speed for cases 3 and 5 that, respectively, have two edge cracks and two inside cracks.

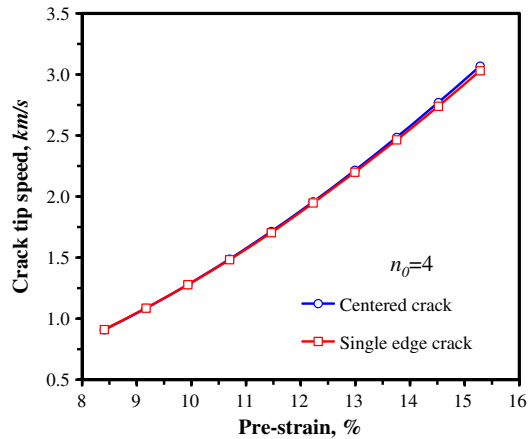


Fig. 10. Dependence of the crack-tip speed upon the axial prestrain.

by Marder and Liu [24], Marder [25] and Bouchbinder et al. [26] who equated it to dynamic analog of lattice trapping. That is, there is a forbidden range of speeds for steady-state crack propagation in crystals at 0 K.

For the axial prestrain of 15.3%, we have plotted in Fig. 9 crack-tip speeds for cases 3 (two edge cracks) and 5 (two interior cracks). In each case, the two cracks start interacting with each other when the distance between them is about $8d$ as exemplified by the slight decrease followed by the dramatic increase in their crack-tip speeds.

In Fig. 10 we have plotted the steady state crack speed as a function of the axial prestrain, ε_0 . A least squares fit to these curves is (correlation coefficient $R^2 = 0.9998$)

$$v = 0.0127\varepsilon_0^2 + 0.0114\varepsilon_0 - 0.0851, \quad 0.008 < \varepsilon_0 < 0.15, \quad (10)$$

where v is in km/s.

We note that cracks with $n_0 = 4$ inserted in the SLGS prestrained to 7.6% did not propagate for all 5 cases studied. Here n_0 equals the number of bonds broken to insert an initial crack. It should be noted that cracks with $n_0 = 4$ propagated in pre-cracked unstrained SLGS for applied axial strains less than 7.6% [13]. Omeltchenko et al. [27] performed MD simulations using the Tersoff–Brenner potential to investigate crack propagation in a graphite sheet consisting of two million atoms. The pristine sheet was pre-strained in tension, and an initial notch was then introduced in it. They reported that the inserted notch of length 30 \AA did not propagate for pre-strains less than 12%.

5. Conclusions

Crack propagation in pre-strained single layer graphene sheets has been studied using MD simulations. Main results of this work are summarized below.

- Crack-tip speeds rapidly reach steady state values which are independent of the initially inserted crack length, its location (in the zigzag direction) and whether one or two cracks are inserted. The steady state crack-tip speed increases with an increase in the value of the prestrain. At a pre-strain of 15.3%, which is just below the failure strain of 15.48%, the steady crack-tip speed equals 3 km/s, and the crack propagation is stable. For a pre-strain of 8.4%, the steady state crack-tip speed equals 0.9 km/s. Cracks do not propagate if the prestrain is less than 7.6%.
- Two cracks on the central horizontal axis of the SLGS start interacting with each other when the distance between their tips equals $8\sqrt{3} r_0$ where r_0 equals the distance between two carbon atoms in the unloaded relaxed configuration.
- The prestrained SLGS exhibits rising J -curve signifying that there is no single value of the critical SERR. Thus a single toughness value cannot be specified.

Acknowledgements

Dr. Minh-Quy Le was supported by the Vietnamese Fulbright visiting scholar program during the academic year 2011–2012, and Professor R.C. Batra was partially supported by the US ONR Grant N00014-11-1-0594 with Dr. Y.D.S. Rajapakse as the Program Manager.

References

- [1] C. Lee, X. Wei, J.W. Kysar, J. Hone, *Science* 321 (2008) 385–388.
- [2] A.A. Balandin, S. Ghosh, W. Bao, I. Calizo, D. Teweldebrhan, F. Miao, C.N. Lau, *Nano Lett.* 8 (2008) 902–907.
- [3] K. Bolotin, K. Sikes, Z. Jiang, M. Klima, G. Fudenberg, J. Hone, P. Kim, H. Stormer, *Solid State Commun.* 146 (9–10) (2008) 351–355.
- [4] S. Stankovich, D.A. Dikin, G.H.B. Dommett, K.M. Kohlhaas, E.J. Zimney, E.A. Stach, R.D. Piner, S.T. Nguyen, R.S. Ruoff, *Nature* 442 (2006) 282–286.
- [5] D. Li, R.B. Kaner, *Science* 320 (2008) 1170–1171.
- [6] Y. Jin, F.G. Yuan, *J. Nanosci. Nanotechnol.* 5 (4) (2005) 601–608.
- [7] M. Xu, A. Tabarraei, J.T. Paci, J. Oswald, T. Belytschko, *Int. J. Fract.* 173 (2) (2012) 163–173.
- [8] X. Wei, B. Fragneaud, C.A. Marianetti, J.W. Kysar, *Phys. Rev. B* 80 (2009) 205407.
- [9] J.R. Rice, *J. Appl. Mech.* 35 (1968) 379–386.
- [10] K. Nakatani, A. Nakatani, Y. Sugiyama, H. Kitagawa, *AIAA J.* 38 (4) (2000) 695.
- [11] Y. Jin, F.G. Yuan, *J. Nanosci. and Nanotechnol.* 5 (12) (2005) 2099–2107.
- [12] R. Khare, S.L. Mielke, J.T. Paci, S. Zhang, R. Ballarini, G.C. Schatz, T. Belytschko, *Phys. Rev. B* 75 (2007) 075412.
- [13] M.Q. Le, R.C. Batra, *Comput. Mater. Sci.* 69 (2013) 381–388.
- [14] S.S. Terdalkar, S. Huang, H. Yuan, J.J. Rencis, T. Zhu, S. Zhang, *Chem. Phys. Lett.* 494 (2010) 218–222.
- [15] Y. Guo, N. Karasawa, W.A. Goddard III, *Nature* 351 (1991) 464–467.
- [16] J.H. Walther, R. Jaffe, T. Halicioglu, P. Koumoutsakos, *J. Phys. Chem. B* 105 (2001) 9980–9987.
- [17] L.A. Girifalco, M. Hodak, R.S. Lee, *Phys. Rev. B* 62 (2000) 13104–13110.
- [18] S.J. Plimpton, *J. Comput. Phys.* 117 (1995) 1–19.
- [19] T. Schneider, E. Stoll, *Phys. Rev. B* 17 (3) (1978) 1302–1322.
- [20] F. Liu, P. Ming, J. Li, *Phys. Rev. B* 76 (2007) 064120.
- [21] M. Xu, J.T. Paci, J. Oswald, T. Belytschko, *Int. J. Solids Struct.* 49 (2012) 2582.
- [22] S.S. Gupta, R.C. Batra, *J. Comput. Theor. Nanosci.* 7 (2010) 2151–2164.
- [23] H. Zhao, K. Min, N.R. Aluru, *Nano Lett.* 9 (8) (2009) 3012.
- [24] M. Marder, X. Liu, *Phys. Rev. Lett.* 71 (1993) 2417–2420.
- [25] M. Marder, *Int. J. Fract.* 130 (2004) 517–555.
- [26] E. Bouchbinder, J. Fineberg, M. Marder, *Annu. Rev. Condens. Matter Phys.* 1 (2010) 371–395.
- [27] A. Omeltchenko, J. Yu, R.K. Kalia, P. Vashishta, *Phys. Rev. Lett.* 78 (11) (1997) 2148–2151.